Infrared signature of active massive black holes in nearby dwarf galaxies[*]

Francine R. Marleau[1], Dominic Clancy[1], Rebecca Habas[1], and Matteo Bianconi[1,2]

[1] Institute of Astro and Particle Physics, University of Innsbruck, Technikerstraße 25, 6020 Innsbruck, Austria
e-mail: [Francine.Marleau;Dominic.Clancy;Rebecca.Habas]@uibk.ac.at
[2] Astrophysics and Space Research Group, School of Physics and Astronomy, University of Birmingham, Edgbaston, Birmingham B15 2TT, UK

ABSTRACT

Context. We investigate the possible presence of active galactic nuclei (AGN) in dwarf galaxies and other nearby galaxies to identify candidates for follow-up confirmation and dynamical mass measurements.

Aims. We identify candidate active central massive black holes (CMBH) using their mid-infrared emission, verify their nature using existing catalogues and optical line emission diagnostics, and study the relationship between their mass and the mass of their host galaxy.

Methods. We use the Wide-field Infrared Survey Explorer (WISE) All-Sky Release Source Catalog and examine the infrared colours of a sample of dwarf galaxies and other nearby galaxies in order to identify both unobscured and obscured candidate AGN by applying the infrared colour diagnostic. Stellar masses of galaxies are obtained using a combination of three independent methods. Black hole masses are estimated using the bolometric luminosity of the AGN candidates and computed for three cases of the bolometric-to-Eddington luminosity ratio.

Results. We identify 303 candidate AGN, of which 276 were subsequently found to have been independently identified as AGN via other methods. The remaining 9% require follow-up observations for confirmation. The activity is detected in galaxies with stellar masses from $\sim 10^6$ to 10^9 $M_\odot$; assuming the candidates are AGN, the black hole masses are estimated to be $\sim 10^3 - 10^6$ $M_\odot$, adopting $L_{\rm bol} = 0.1$ $L_{\rm Edd}$. The black hole masses probed are several orders of magnitude smaller than previously reported for centrally located massive black holes. We examine the stellar mass versus black hole mass relationship in this low galaxy mass regime. We find that it is consistent with the existing relation extending linearly (in log-log space) into the lower mass regime.

Conclusions. These findings suggest that CMBH are present in low-mass galaxies and in the Local Universe, and provide new impetus for follow-up dynamical studies of quiescent black holes in local dwarf galaxies.

Key words. galaxies: general – galaxies: Seyfert – galaxies: active – galaxies: dwarf – Local Group – infrared: galaxies

1. Introduction

Following pioneering work in the late 1960s (Zel'dovich & Novikov 1965; Salpeter 1964; Lynden-Bell 1969; Bardeen 1970; Lynden-Bell & Rees 1971), a paradigm has gradually emerged in which central massive black holes (CMBH) have come to be regarded as an integral component of "most, if not all, massive galaxies", intimately linked to their formation and evolution (Merritt & Ferrarese 2001; Bender & Kormendy 2003; Ho et al. 2000; Peterson 2008; Peterson et al. 2010; Heckman & Kauffmann 2011; Schawinski 2012; Kormendy & Ho 2013). However, despite a great deal of research and progress on many fronts towards a better understanding of this paradigm (see e.g. Merloni 2015, for a recent review), essentially all of the fundamental questions concerning the formation, growth, and host co-evolution of CMBH remain unanswered. One such question, which is the focal point of this article, is whether CMBH are generic to all galaxies. It is interesting to note that while it is often stated in the literature that black holes are to be found at

the centres of most galaxies, until recently there has been insufficient evidence to support this claim, even for the case of massive galaxies not possessing a significant bulge component, let alone the general population of galaxies, most of which are not massive. In other words, it is not generally known whether CMBH are only a generic feature of certain galaxy types, present only in galaxies above a certain mass threshold, or subject to a combination of both of these restrictions.

The question of CMBH genericity is strongly related to the issues of formation, growth and galaxy co-evolution. Its relationship with the subject of galaxy formation can be understood by considering the current observational constraints on high-redshift quasars (e.g. Fan 2001; Mortlock et al. 2011; Wu et al. 2015; Matsuoka et al. 2016), which imply that CMBH were present at very early times ($z > 7$) and therefore must have formed either concurrently with their host galaxies or prior to them. While these constraints clearly highlight the close connection between the formation of CMBH and their hosts, they also conversely imply that galaxies which do not host a CMBH will likely have undergone distinct formation processes. Similarly, in order to understand the link between CMBH genericity and evolution, one need only consider the evidence of the significant

---

effects that active galactic nuclei (AGN) have on their hosts' evolutions (Silk & Rees 1998; King 2003; Fabian 2012; Silk 2013; Ishibashi & Fabian 2014) in order to realise that galaxies which do not host CMBH may have undergone a markedly different evolution from those that do.

It is apparent from these simple observations that the question of CMBH genericity has important implications for the theory and modelling of galaxy and large-scale structure evolution (see e.g. Benson 2010; Silk 2013, for recent reviews). Indeed, the importance of modelling AGN feedback has been understood for some time (Springel et al. 2005; Di Matteo et al. 2005; McNamara & Nulsen 2007) and various approaches are now incorporated as standard in simulations of galaxy and structure evolution (Sijacki et al. 2007; Di Matteo et al. 2008; Khalatyan et al. 2008; Booth & Schaye 2009; Poweret et al. 2011; DeGraf et al. 2012; Newton & Kay 2013). Feedback from AGN has also been shown to play a significant role up to the largest scales of structure Haider et al. (2016; see also Wurster & Thacker 2013, for a comparison of models). In general, it is expected that theories and models which assume that black holes are generic will differ significantly in their predictions from those that do not. For example, while most models and simulations at present include the effects of AGN feedback from massive galaxies, including the effects of AGN feedback from low-mass galaxies may account for the observed low baryon fraction in Milky Way-type galaxies at the present epoch (see e.g. Peirani et al. 2012).

While the broad question of the genericity of CMBH remains open, recent findings have been strongly supportive of CMBH being generic for the subset of massive galaxies, i.e. for galaxies with stellar masses above $\sim 10^9 M_\odot$. In particular, in a recent work Marleau et al. (2013) studied a sample of 15 991 galaxies and found the fraction of galaxies containing a CMBH to be approximately the same for each morphological type. This study was itself prompted by the recent discovery of CMBH in galaxies lacking any substantial spheroidal component (Reines et al. 2011; Simmons et al. 2013). Prior to this there was only strong evidence for the generic presence of CMBH in galaxies with a significant bulge component (Kormendy & Richstone 1995; Magorrian et al. 1998; Ferrarese & Merritt 2000; Gebhardt et al. 2000; Kormendy & Ho 2013). While evidence continues to accrue to firmly establish the generic existence of CMBH within massive galaxies, attention has now begun to shift to the question of whether CMBH are also generic in the low-mass regime, i.e. in galaxies with stellar masses below $\sim 10^9 M_\odot$, or in other words, whether CMBH are generic to dwarf galaxies.

Until very recently it was not even known whether any dwarf galaxies contained CMBH, let alone whether they were generic. However, during the last few years results in this area have been rapid. It is now known that a significant number of galaxies with masses $\sim 10^9 - 10^{10} M_\odot$, i.e. at the high end of the dwarf galaxy mass regime and the low end of the massive galaxy regime, likely contain active CMBH. In particular, Moran et al. (2014), Reines et al. (2013, 2014), Barth et al. (2008), Greene et al. (2007, 2004), Dong et al. (2012 and 2007) have detected the optical signatures of mainly unobscured (type 1) AGN in 768 galaxies with total stellar masses in the range $\sim 10^8 - 10^{11} M_\odot$, while Marleau et al. (2013) have identified the first mid-infrared signatures of both obscured and unobscured candidate AGN in 73 dwarf galaxies with masses in the range $\sim 10^7 - 10^9 M_\odot$.

Even though these findings are encouraging, they barely probe the dwarf galaxy mass range, and it is also the case that the black hole masses derived from the optical spectra may be subject to large systematic uncertainties. Additionally, one would ideally also like to have dynamically derived masses. At the present time, there is only one dynamical measurement of a black hole in a galaxy classified as a dwarf galaxy, i.e. with a mass below $3 \times 10^9 M_\odot$, namely the CMBH in NGC 4395, which has a mass of $4 \times 10^5 M_\odot$ (den Brok et al. 2015). Additionally, Seth et al. (2014) found a black hole of mass $2.1 \times 10^7 M_\odot$ in the ultra-compact dwarf galaxy M 60-UCD1 of total stellar mass $1.2 \times 10^8 M_\odot$, though this is believed to be a tidally stripped galaxy whose progenitor had a mass of $\sim 10^{10} M_\odot$, which would then be consistent with the known black hole mass to host total stellar mass scaling relation (Marleau et al. 2013).

As dwarf galaxies exhibit a number of properties that differentiate them from other galaxies (see review in Mateo 1998) and are known to have different evolutionary histories from massive galaxies, this could be a consequence of them not having CMBH or of having a different relationship with their CMBH. If it is the case that dwarf galaxies generically contain CMBH, it is therefore not necessarily the case that what has been learned about the relationships between CMBH and their hosts in the massive regime, as exhibited in their scaling relations, will necessarily hold for dwarf galaxies. However, the extension of current scaling relations suggests that dwarf galaxies should host an intermediate mass CMBH, if they host one at all. The low surface brightness of dwarfs necessitates studying them in the nearby Universe; consequently, this population of galaxies provides the opportunity to discover very nearby, low-mass CMBH ($< 10^6 M_\odot$), which would be ideal for follow-up dynamical studies.

Motivated by our recent infrared (IR) study of active massive black holes in galaxies of all morphological types (Marleau et al. 2013) and wide range of stellar masses, we have undertaken a census in the very nearby Universe, specifically targeting low-mass dwarf systems that should be ideal hosts for CMBH in the mass range of intermediate mass black holes (IMBH; $M_{BH} \sim 10^3 - 10^6 M_\odot$). Additionally, we are interested in detecting AGN in nearby galaxies regardless of their mass so that we can identify targets for future dynamical mass measurement. The structure of our paper is as follows. In Sect. 2, we describe our dwarfs and other nearby galaxies sample. In Sects. 3 and 4, this sample is matched to an infrared catalogue and the AGN candidates are identified using the infrared colour diagnostic. The detection of these AGN are verified using existing catalogues and optical line emission diagnostic in Sect. 5 and their distance distribution is presented in Sect. 6. In Sects. 7 and 8, we derive stellar masses for the host galaxies of our AGN candidates and compute the AGN fraction as a function of stellar mass based on our AGN selection method. In Sects. 9 and 10, we evaluate the black hole masses for our AGN candidates, present the black hole mass versus stellar mass scaling relation, and compare our black hole mass estimates to those derived using other methods. In Sect. 11, we discuss and summarize our results. We believe that by firmly establishing the presence of active IMBHs not only at the low end of the galaxy mass function but also in the nearby Universe, it will be possible to follow-up their quiet counterparts with dynamical studies and hence provide further support for their existence.

2. Nearby galaxy sample

Our primary sources were selected from the Updated Nearby Galaxy Catalogue of Karachentsev et al. (2013) and the catalogue of Local Group (LG) galaxies of McConnachie et al. (2012). The first is a recently updated all-sky catalogue

Table 1. Sample descriptions and sizes.

Name	Content	Size
Primary sample	Catalogue of Karachentsev et al. (2013);	5143
	catalogue of McConnachie et al. (2012);	
	NED dwarfs, E peculiar, compact E	
MRBGD samples	Catalogues from MRBGD	754
Total sample	Primary and MRBGD	5897
WISE sample	WISE matches to Primary sample	5042
WISE S/N sample	WISE matches to Primary sample with $S/N > 3$	3326
WISE MRBGD AGN sample	WISE matches to MRBGD NL+BL AGN with $S/N > 3$	700[a]
WISE MRBGD BL AGN sample	WISE matches to MRBGD BL AGN with $S/N > 3$	549[a]
WISE MRBGD NL AGN sample	WISE matches to MRBGD NL AGN with $S/N > 3$	152[a]
WISE BCD AGN sample	WISE matches to BCD AGN with $S/N > 3$	182
WISE Griffith AGN sample	WISE matches to Griffith AGN with $S/N > 3$	2
IR selected AGN sample	WISE S/N sample with $W1 - W2 > 0.5$	303
IR new selected AGN sample	IR selected AGN sample NOT in the MRBGD NL+BL AGN sample	43
IR selected BCD AGN sample	WISE BCD AGN sample with $W1 - W2 > 0.5$	18
IR selected MRBGD AGN sample	WISE MRBGD NL+BL AGN sample with $W1 - W2 > 0.5$	258[a]
IR selected MRBGD BL AGN sample	WISE MRBGD BL AGN sample with $W1 - W2 > 0.5$	245[a]
IR selected MRBGD NL AGN sample	WISE MRBGD NL AGN sample with $W1 - W2 > 0.5$	15[a]
IR selected Griffith AGN sample	WISE Griffith AGN sample with $W1 - W2 > 0.5$	2
IR new selected AGN sample with other AGN diagnostic	IR selected new AGN sample with other AGN diagnostic	16
IR selected AGN sample also identified as AGN via other methods	adding four samples above	276[a]
IR selected AGN sample with redshift/distance	IR selected AGN sample with redshift/distance	300
IR selected new AGN sample with redshift/distance	IR selected new AGN sample with redshift/distance	40
WISE S/N sample in MPH/JHU catalogue	WISE S/N sample with MPH/JHU catalogue matches	968
WISE S/N sample in BPT diagram	WISE S/N sample with MPH/JHU BPT emission line fluxes	954
WISE S/N sample with stellar masses	WISE S/N sample with MPH/JHU stellar masses	934
IR selected AGN sample with stellar masses	IR selected AGN sample with MPH/JHU stellar masses	264
IR selected dwarf AGN sample	IR selected AGN sample with log $M_{stellar} < 9.5$	62
IR selected AGN sample with stellar masses and redshift/distance	IR selected AGN sample with MPH/JHU stellar masses and redshift/distance	264
IR selected MRGBD AGN sample with stellar masses and redshift/distance	IR selected BL+NL AGN sample with MPH/JHU stellar masses and redshift/distance	239[a]
IR selected MRGBD BL AGN sample with stellar masses and redshift/distance	IR selected BL AGN sample with MPH/JHU stellar masses and redshift/distance	227[a]
IR selected MRGBD NL AGN sample with stellar masses and redshift/distance	IR selected NL AGN sample with MPH/JHU stellar masses and redshift/distance	14[a]
IR selected Griffith AGN sample with stellar masses and redshift/distance	IR selected Griffith AGN sample with MPH/JHU stellar masses and redshift/distance	2
IR selected new AGN sample with stellar masses and redshift/distance	IR selected new AGN sample with MPH/JHU stellar masses and redshift/distance	23
IR selected NED BCD AGN sample with stellar masses and redshift/distance	IR selected NED BCD AGN sample with MPH/JHU stellar masses and redshift/distance	15
IR selected AGN sample in BPT diagram	IR selected AGN sample with MPH/JHU BPT emission line fluxes	135
IR selected MRBGD AGN sample in BPT diagram	IR selected MRBGD NL+BL AGN sample with MPH/JHU BPT emission line fluxes	126[a]
IR selected MRBGD NL AGN sample in BPT diagram	IR selected MRBGD BL AGN sample with MPH/JHU BPT emission line fluxes	111[a]
IR selected MRBGD BL AGN sample in BPT diagram	IR selected MRBGD NL AGN sample with MPH/JHU BPT emission line fluxes	16[a]
IR selected new AGN sample in BPT diagram	IR selected new AGN sample with MPH/JHU BPT emission line fluxes	9
IR selected NED BCD AGN sample in BPT diagram	IR selected NED BCD AGN sample with MPH/JHU BPT emission line fluxes	83
IR selected AGN sample with IR and [OIII] $\lambda5007$ BH masses	IR selected AGN sample with IR BH masses and [OIII] $\lambda5007$ BH masses	248

Notes. [a] Two objects in this sample are classified as both NL and BL.

containing 869 nearby galaxies with distance estimates within 11 Mpc or corrected radial velocities less than 600 km s^{-1}. The latter contains all known galaxies with distances determined from measurements of resolved stellar populations that place them within 3 Mpc of the Sun. We also searched the NASA Extragalactic Database (NED) under the following three classifications: dwarfs (dwarf, nucleated, dwarf elliptical (dE), dwarf lenticular (S0), dwarf spiral (dS), dwarf irregular (dI) and blue compact dwarf (BCD)); E peculiar; and compact E. Dwarfs are ill defined in the literature (see e.g. Dunn 2010, for a review on the various definitions), and some known dwarfs, such as NGC 185 and 147, are labelled in NED as elliptical galaxies. Thus, we expanded our search parameters to ensure that we did not lose any potential dwarfs in the nearby Universe. Dwarf spirals are a contentious subject in and of themselves, and we did not search NED for spiral galaxies to add to the sample. In order to define our dwarf sample in a consistent manner – regardless of their previous classification in the literature – in the following work, we apply our own mass cut (see Sects. 4 and 7).

This primary sample was augmented by the surveys of galaxies, including dwarfs at the high end of the mass range, that had already been identified as having the optical spectroscopic signature of low-mass actively accreting black holes (Moran et al. 2014; Reines et al. 2013, 2014; Barth et al. 2008; Greene et al. 2007, 2004; Dong et al. 2012, 2007, hereafter MRBGD). These AGN candidates will be used to verify the IR selection technique. The final list, cleaned of all duplicates, consists of a total of 5897 galaxies (see Table 1 for a summary of the various samples and their sizes discussed throughout this paper).

3. Mid-infrared colours of nearby galaxies

For this work, we used mid-infrared colours to identify the AGN in our sample. One advantage of using images in the mid-infrared is that both unobscured (type 1) and obscured (type 2) AGN are detected. The mid-infrared selection of unobscured AGN relies upon distinguishing the approximately power-law AGN spectrum from the black-body stellar spectrum of galaxies (which peaks at rest-frame 1.6 μm; Assef et al. 2010, Fig. 3) using its red mid-infrared colours. It is important to note that most of the previous surveys of AGN in dwarf galaxies have been carried out in the optical. Optical studies are biased towards observing primarily type 1 AGN, even though the unified
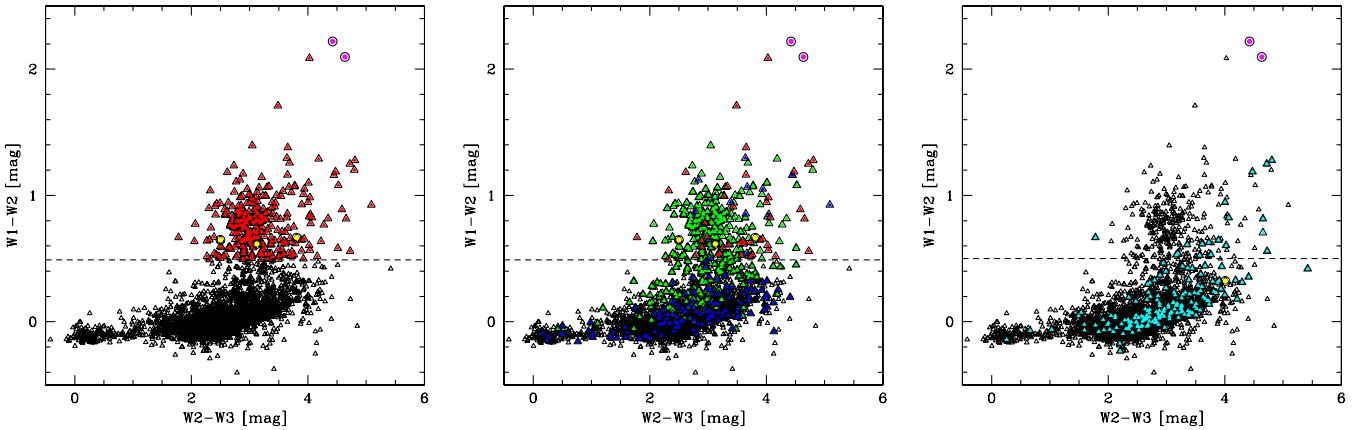
Fig. 1. *Left*: $W1 - W2$ colour vs. $W2 - W3$ colour of our 3326 target galaxies (black open triangles). The 303 sources above our IR colour cut are shown as red filled triangles. The two outliers with very red colours in the top right-hand corner of the diagram (magenta filled circles) are the low-metallicity and heavily obscured BCDs that were originally identified by Griffith et al. (2011). The two famous dwarf Seyfert 1 galaxies (NGC 4395 and POX 52), as well as a Seyfert 1 galaxy hosting a low-mass BH (UM 625; yellow filled circles), have WISE colours above our selection cut-off. *Middle*: same as left, but showing the AGN that have been previously identified in the MRBGD optical samples split into 549 type 1 (BL; green filled triangles) and 152 type 2 (NL; blue filled triangles). Although a large fraction of these optically identified AGN fall in our IR selected sample of 303 galaxies, many also have WISE colours below our selection cut-off (dashed line). The 43 candidate AGN, selected using the IR diagnostic, that are not in the samples of MRBGD are shown as red filled triangles. *Right*: same as left, but showing the 182 BCDs (cyan filled triangles) and the 2 low-metallicity and heavily obscured BCDs that were originally identified by Griffith et al. (2011; magenta filled circles). The BCD MRK 709 S (yellow filled circle), one of the most metal-poor BCDs with evidence of an active galactic nucleus (Reines et al. 2014), also has a WISE colour below our selection cut-off.

AGN model (Antonucci 1993; Urry & Padovani 1995) predicts that type 2 AGN should outnumber type 1 by a factor of ∼3 (e.g., Comastri et al. 1995; Treister et al. 2004; Ballantyne et al. 2011). Another advantage to working with mid-infrared data is that they allow AGN to be easily distinguished from stars and galaxies.

The infrared magnitudes of our galaxies were obtained from the Wide-field Infrared Survey Explorer (WISE; Wright et al. 2010) All-Sky Release Source Catalog. This catalogue contains positions and photometry at 3.4 ($W1$), 4.6 ($W2$), 12 ($W3$) and 22 ($W4$) μm for 563, 921, 584 point-like and resolved objects detected on the Atlas Intensity images. The photometry in this catalogue was performed using point source profile-fitting and multi-aperture photometry and the estimated sensitivities are 0.068, 0.098, 0.86 and 5.4 mJy (5σ) at 3.4, 4.6, 12 and 22 μm in unconfused regions on the ecliptic plane. J2000 positions and uncertainties were reconstructed using the 2MASS Point Source Catalog as astrometric reference. Astrometric accuracy is approximately 0.2 arcsec root-mean-square on each axis with respect to the 2MASS reference frame for sources with signal-to-noise ratio (S/N) greater than forty.

We cross-matched our nearby galaxy catalogue with the WISE All-Sky Release Source Catalog using the US Virtual Astronomical Observatory (VAO) cross-comparison tool. Using a matching radius of 6 arcsec, corresponding to the resolution of WISE in W1, we obtained 5042 matches. For each of the galaxies, WISE photometry for W1, W2, W3 and W4 was gathered and a S/N cut of 3 was imposed on the first three bands since only these three bands are needed for the AGN diagnostic diagram and to obtain an estimate of the BH mass (see Sect. 9). We used the point source profile-fitting photometry (w1mpro, w2mpro, w3mpro and w4mpro) for sources with goodness-of-fit ≤3.0 which indicates that the source shape is consistent with a point source and the source is not associated with or superimposed on a 2MASS Extended Source Catalog (XSC) source.

For sources with goodness-of-fit >3.0, we used the 5.5 arcsec radius aperture photometry (w1mag_1, w2mag_1, w3mag_1 and w4mag_1) to measure the IR colours. Using the three photometric bands, two photometric colours were determined. In Fig. 1, we plot the $W1-W2$ versus $W2-W3$ colour for the 3326 galaxies in our final $S/N > 3$ WISE matched sample.

4. Infrared colour diagnostic for AGN candidates

Several mid-infrared colour diagnostics have been used in the literature to select AGN, starting with the pioneering work of (Lacy et al. 2004, 2007) and the so-called "Lacy wedge". For low redshift galaxies (i.e. $z < 1.3$), which applies to our sample of nearby galaxies, Stern et al. (2012) show that WISE is able to robustly identify AGN using the more sensitive W1 (3.4 μm) and W2 (4.6 μm) bands alone. According to these authors, a colour cut of $W1 - W2 > 0.8, 0.7, 0.6$, and 0.5 is able to identify AGN with a reliability of 95%, 85%, 70% and 50%, respectively. Note that although reliability drops with lower colour cut, completeness increases and reaches the 95% level for $W1 - W2 > 0.5$. As can be seen in their Fig. 2, even the least stringent colour cut of $W1 - W2 > 0.5$ identifies galaxies in which the AGN fraction is ≥50% to $z = 0.5$ (this fraction changes depending on extinction). This means that this colour cut only identifies AGN that dominate the emission from their host galaxies. For galaxies in which the AGN do not dominate over the host galaxy emission, dilution of the mid-infrared AGN continuum by the host galaxy light can cause bluer $W1-W2$ colours that become indistinguishable from star-forming galaxies. In fact, as is shown in Sect. 5.2, a large fraction of the optically identified AGN in the Sloan Digital Sky Survey (SDSS) galaxy samples of MRBGD have $W1 - W2$ colours below this cut-off.

The 3326 galaxies with WISE matches and $S/N > 3$ in $W1$, $W2$ and $W3$ are shown in Fig. 1, left. With our colour cut of $W1 - W2 > 0.5$, we identify 303 candidate AGN (see Fig. 2). These final numbers come after we conservatively removed candidates
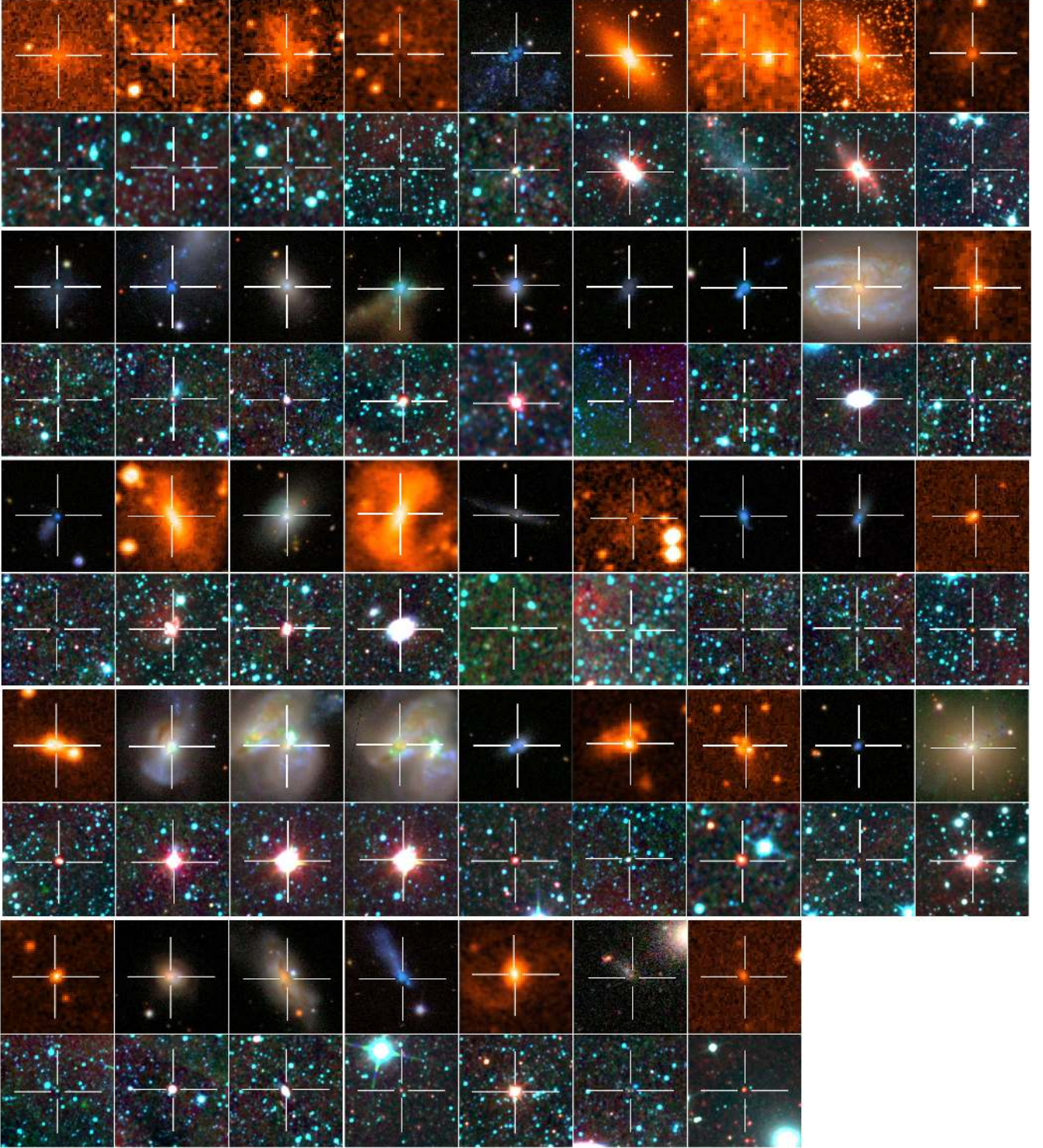
Fig. 2. Mosaic of the 43 candidate AGN, selected using the IR diagnostic, which are not in the samples of MRBGD. They are ordered, *from left* to *right* and *top* to *bottom*, by increasing distance with the exception of the first three candidates, which have no known redshift/distance (see Table 2). The *top images* are either optical g', r', i' colour images from SDSS, which are 76.8″ on a side (except for OBJ 36, which is 153″ on a side), or false colour images from the DSS-2-red catalogue, which are 1′ on a side (except for OBJ 6 and 8, which are 4′ on a side). The *bottom images* are W1, W2, W3 colour images from WISE, ~9′ on a side (except for OBJ 14, 23 and 34, which are ~4′ on a side).

that were found close to an image artefact that could possibly contaminate the source and give an erroneous photometry. Of the 303 candidate AGN, 62 are classified as dwarf galaxies based on a log $M_{stellar}$ cut of 9.5 (similar to Reines et al. 2013). The list of these galaxies, ordered by increasing distance, can be found in Tables 2 (dwarfs) and 3 (non-dwarfs).

In our analysis, we use the colour cut of $W1 - W2 > 0.5$, without imposing any $W2 - W3$ colour restriction. One cause for possible concern when using this cut is the contamination of low metallicity star-forming galaxies. The effect of metallicity on the intensity of the polycyclic aromatic hydrocarbon (PAH) emission has been quantified in detail

Table 2. Dwarf galaxies with IR signatures of active massive black holes.

Name	RA J2000	Dec J2000	Redshift	Distance Mpc	$\log(M_{\rm stellar})$ $M_\odot$	$W1 - W2$ [mag]	$W2 - W3$ [mag]	$\log(M_{\rm BH\,IR})$ $M_\odot$	Image
AM 1906-621	$19^{\rm h}11^{\rm m}33.43^{\rm s}$	$-62^{\rm d}10^{\rm m}22.4^{\rm s}$	–	–	–	0.784	2.950	–	1
AM 1238-405	$12^{\rm h}41^{\rm m}15.40^{\rm s}$	$-41^{\rm d}09^{\rm m}34.0^{\rm s}$	–	–	–	0.628	3.626	–	2
ESO 184- G 050	$19^{\rm h}16^{\rm m}17.23^{\rm s}$	$-54^{\rm d}20^{\rm m}40.8^{\rm s}$	–	–	–	0.586	3.252	–	3
HIPASS J1247-77	$12^{\rm h}47^{\rm m}32.60^{\rm s}$	$-77^{\rm d}35^{\rm m}01.0^{\rm s}$	0.001378	3.160	–	2.086	4.026	2.192	4
UGC 04459	$08^{\rm h}34^{\rm m}07.20^{\rm s}$	$+66^{\rm d}10^{\rm m}54.0^{\rm s}$	0.000067	3.253	–	1.379	3.654	2.687	5
NGC 5253	$13^{\rm h}39^{\rm m}55.80^{\rm s}$	$-31^{\rm d}38^{\rm m}24.0^{\rm s}$	0.001358	3.646	–	1.710	3.487	5.602^a	6
IC 2574	$10^{\rm h}28^{\rm m}23.48^{\rm s}$	$+68^{\rm d}24^{\rm m}43.7^{\rm s}$	0.000190	3.835	–	0.646	2.885	1.638	7
NGC 4395	$12^{\rm h}25^{\rm m}48.86^{\rm s}$	$+33^{\rm d}32^{\rm m}48.7^{\rm s}$	0.001064	4.491	7.156	0.648	2.500	3.589	–
HIPASS J1337-39	$13^{\rm h}37^{\rm m}25.10^{\rm s}$	$-39^{\rm d}53^{\rm m}52.0^{\rm s}$	0.001641	4.800	–	0.888	4.583	2.506	9
UGC 07544	$12^{\rm h}26^{\rm m}37.74^{\rm s}$	$+62^{\rm d}22^{\rm m}47.2^{\rm s}$	0.002372	9.499	6.728	0.590	2.902	2.569	10
MRK 0094	$08^{\rm h}37^{\rm m}43.48^{\rm s}$	$+51^{\rm d}38^{\rm m}30.3^{\rm s}$	0.002451	9.817	5.980	0.816	4.655	3.839	11
UGC A298	$12^{\rm h}46^{\rm m}55.40^{\rm s}$	$+26^{\rm d}33^{\rm m}51.0^{\rm s}$	0.002743	9.950	8.175	0.519	3.730	4.758	12
UGC A116	$05^{\rm h}55^{\rm m}42.60^{\rm s}$	$+03^{\rm d}23^{\rm m}32.0^{\rm s}$	0.002632	10.300	7.286	1.278	4.806	5.746	13

Notes. Column (1): object name. Columns (2) and (3); right ascension and declination (J2000). Column (4): redshift. Column (5): distance in Mpc. Column (6): log of host galaxy stellar mass measured from SED fit. Columns (7) and (8): WISE colours. Column (9): log of central black hole mass estimates based on IR luminosity (assuming $L_{\rm bol} = 0.1\,L_{\rm Edd}$). Column (10): image number in Fig. 2. $^{(a)}$ These sources are extended and larger than the largest WISE aperture (24.75 arcsec radius aperture); therefore, the infrared black hole mass estimates for these sources are only lower limits. The full table is available at the CDS. A portion is shown here for guidance regarding its form and content.

Table 3. Non-dwarf galaxies with IR signatures of active massive black holes.

Name	RA J2000	Dec J2000	Redshift	Distance Mpc	$\log(M_{\rm stellar})$ $M_\odot$	$W1 - W2$ [mag]	$W2 - W3$ [mag]	$\log(M_{\rm BH\,IR})$ $M_\odot$	Image
CIRCINUS	$14^{\rm h}13^{\rm m}09.30^{\rm s}$	$-65^{\rm d}20^{\rm m}21.0^{\rm s}$	0.001448	4.207	–	1.038	2.325	6.306^a	8
NGC 2964	$09^{\rm h}42^{\rm m}54.23^{\rm s}$	$+31^{\rm d}50^{\rm m}50.6^{\rm s}$	0.004430	20.429	10.201	0.667	1.780	6.497^a	17
NGC 4194	$12^{\rm h}14^{\rm m}09.47^{\rm s}$	$+54^{\rm d}31^{\rm m}36.6^{\rm s}$	0.008178	39.100	9.684	0.531	3.761	7.235^a	29
NGC 3690 NED01	$11^{\rm h}28^{\rm m}31.02^{\rm s}$	$+58^{\rm d}33^{\rm m}40.7^{\rm s}$	0.009990	40.240	10.357	1.183	2.617	7.877^a	30
NGC 3690 NED02	$11^{\rm h}28^{\rm m}33.63^{\rm s}$	$+58^{\rm d}33^{\rm m}46.6^{\rm s}$	0.010456	42.133	10.461	0.983	4.036	7.864^a	31
Moran08	$10^{\rm h}05^{\rm m}51.19^{\rm s}$	$+12^{\rm d}57^{\rm m}40.6^{\rm s}$	0.009375	43.300	9.777	1.124	2.838	6.466	–
NGC 1275	$03^{\rm h}19^{\rm m}48.16^{\rm s}$	$+41^{\rm d}30^{\rm m}42.1^{\rm s}$	0.017559	68.180	11.067	0.911	3.429	7.752^a	36
Greene137+Dong164	$11^{\rm h}53^{\rm m}41.77^{\rm s}$	$+46^{\rm d}12^{\rm m}42.2^{\rm s}$	0.024251	98.744	10.329	0.518	2.270	6.576	–
Dong222	$14^{\rm h}00^{\rm m}40.57^{\rm s}$	$-01^{\rm d}55^{\rm m}18.3^{\rm s}$	0.025049	102.052	9.661	0.665	3.809	6.678	–
Greene47	$08^{\rm h}24^{\rm m}43.28^{\rm s}$	$+29^{\rm d}59^{\rm m}23.5^{\rm s}$	0.025420	103.594	9.674	1.171	2.888	7.379	–
Reines3NL	$03^{\rm h}22^{\rm m}24.64^{\rm s}$	$+40^{\rm d}11^{\rm m}19.8^{\rm s}$	0.026084	106.352	9.565	0.854	3.647	5.988	–
MRK 0315	$23^{\rm h}04^{\rm m}02.62^{\rm s}$	$+22^{\rm d}37^{\rm m}27.5^{\rm s}$	0.027278	111.319	10.854	0.527	2.796	7.259	38
Greene203	$15^{\rm h}59^{\rm m}09.62^{\rm s}$	$+35^{\rm d}01^{\rm m}47.4^{\rm s}$	0.031024	126.958	10.600	0.743	2.338	7.279^a	–

Notes. Column (1): name. Columns (2) and (3); right ascension and declination (J2000). Column (4): redshift. Column (5): distance in Mpc. Col. (6): log of stellar mass measured from SED fit. Columns (7) and (8): WISE colours. Column (9): log of central black hole mass estimates based on IR luminosity (assuming $L_{\rm bol} = 0.1\,L_{\rm Edd}$). Column (10): image number in Fig. 2. $^{(a)}$ These sources are extended and larger than the largest WISE aperture (24.75 arcsec radius aperture); therefore, the infrared black hole mass estimates for these sources are only lower limits. The full table is available at the CDS. A portion is shown here for guidance regarding its form and content.

using *Spitzer* data (e.g. Calzetti 2011, and references therein). Analyses of galaxies with a range of metallicities show that a factor of ~10 decrease in metallicity is accompanied by an order of magnitude decrease in the 8 μm to total infrared luminosity (i.e. redder $W2 - W3$ colours), with a transition at $12 + \log({\rm O/H}) \approx 8.1$ (Boselli et al. 2004; Madden et al. 2006; Engelbracht et al. 2005; Hogg et al. 2005; Galliano et al. 2005, 2008; Rosenberg et al. 2006; Wu et al. 2006; Draine et al. 2007; Engelbracht et al. 2008; Gordon et al. 2008; Muñoz-Mateos et al. 2009; Marble et al. 2010). Based on the galaxy mass-metallicity relation (Ma et al. 2016), this metallicity transition corresponds to a stellar mass of $\log M_{\rm stellar} \sim 8.0$. Hence many dwarfs, based on our mass cut-off ($\log M_{\rm stellar} = 9.5$), are not expected to have such low metallicity or redder $W2 - W3$ colours. The zero-point of the mass-metallicity relation changes with redshift, so the colours of low-metallicity dwarfs becomes more of an issue as one moves to higher redshifts.

In addition to the confusion between star-forming low-metallicity galaxies and AGN, there is growing evidence that nuclear star clusters can coincide with central massive black holes (e.g. den Brok et al. 2015; Georgiev et al. 2016). In the case of NGC 4395, the $4 \times 10^5\,M_\odot$ central black hole is embedded in a nuclear star cluster of mass $2 \times 10^6\,M_\odot$ (den Brok et al. 2015), and is detected via its infrared signature (Satyapal et al. 2014). Hence, strong levels of star formation do not negate the possible presence and IR detection of an AGN.

If we were to apply a cut on the $W2 - W3$ colour to avoid the redder objects, e.g. a cut with $W2 - W3 < 4.2$ (similar to Eq. (1) of Jarrett et al. 2011), in addition to our $W1 - W2$ cut, we would reject 16 AGN candidates (see Fig. 1). Of these, 2 are the low-metallicity and heavily obscured BCDs that were originally identified by Griffith et al. (2011), but 8 are either type 1 (2) or type 2 (6) optically identified AGN. We note that the remaining 6 that were not previously identified as AGN have colours

Table 4. 16 known AGN with IR signatures of active massive black holes.

Name	RA J2000	Dec J2000	Classification	$\log(M_{\text{BH IR}})$ $M_\odot$	$\log(M_{\text{BH}})$ $M_\odot$	Reference
NGC 5253	$13^{\text{h}}39^{\text{m}}55.80^{\text{s}}$	-31d38m24.0s	Sy2	5.602^a	–	Koulouridis (2014)
CIRCINUS	$14^{\text{h}}13^{\text{m}}09.30^{\text{s}}$	-65d20m21.0s	Sy2	6.306^a	6.23	McConnell et al. (2013)
NGC 2964	$09^{\text{h}}42^{\text{m}}54.23^{\text{s}}$	$+31$d50m50.6s	–	6.497^a	7.34;6.11	Beifiori et al. (2012)
ESO 060- G 019	$08^{\text{h}}57^{\text{m}}26.72^{\text{s}}$	-69d03m36.3s	–	6.015^a	7.83	Davis et al. (2014)
IC 1953	$03^{\text{h}}33^{\text{m}}41.87^{\text{s}}$	-21d28m43.1s	–	5.990^a	7.33	Davis et al. (2014)
NGC 4194	$12^{\text{h}}14^{\text{m}}09.47^{\text{s}}$	$+54$d31m36.6s	AGN	7.235^a	–	SIMBAD info page
NGC 3690 NED01	$11^{\text{h}}28^{\text{m}}31.02^{\text{s}}$	$+58$d33m40.7s	Sy2	7.877^a	7.52	Alonso-Herrero et al. (2014)
NGC 3690 NED02	$11^{\text{h}}28^{\text{m}}33.63^{\text{s}}$	$+58$d33m46.6s	LINER	7.864^a	7.48;8.85	Alonso-Herrero et al. (2014); Zhao et al. (1997)
IRAS 11485-2018	$11^{\text{h}}51^{\text{m}}11.60^{\text{s}}$	-20d36m02.0s	AGN	5.591	–	Sargsyan et al. (2011)
NGC 1275	$03^{\text{h}}19^{\text{m}}48.16^{\text{s}}$	$+41$d30m42.1s	LINER;Sy1	7.752^a	9.28;8.51	McKernan et al. (2010); Panessa et al. (2006)
POX052	$12^{\text{h}}02^{\text{m}}56.91^{\text{s}}$	-20d56m02.7s	Sy1	5.597	5.2	Barth et al. (2004)
MRK 0315	$23^{\text{h}}04^{\text{m}}02.62^{\text{s}}$	$+22$d37m27.5s	Sy1	7.259	–	Veron-Cetty & Vernon (2010)
UGC 04211	$08^{\text{h}}04^{\text{m}}46.38^{\text{s}}$	$+10$d46m36.2s	Sy2	7.156	–	Veron-Cetty & Vernon (2010)
SBS 1415+437	$14^{\text{h}}17^{\text{m}}01.41^{\text{s}}$	$+43$d30m05.5s	QUASAR	5.934	–	Bukhmastova (2001)
ESO 253- G 003	$05^{\text{h}}25^{\text{m}}18.08^{\text{s}}$	-46d00m21.0s	Sy2	8.090^a	–	Veron-Cetty & Vernon (2010)
FCSS J033846.0-352252	$03^{\text{h}}38^{\text{m}}45.97^{\text{s}}$	-35d22m52.3s	Sy2	7.281	–	Veron-Cetty & Vernon (2010)

Notes. In Col. (5), $M_{\text{BH IR}}$ denotes the central black hole mass estimates based on IR luminosity (assuming $L_{\text{bol}} = 0.1\,L_{\text{Edd}}$), while in Col. (6), M_{BH} refers to the central black hole mass estimates based on other conventional (non-infrared) methods. [a] These sources are extended and larger than the largest WISE aperture (24.75 arcsec radius aperture); therefore, the infrared black hole mass estimates for these sources are only lower limits.

similar to these 8 optically identified AGN and hence are valid candidate AGN. We also note that AGN detected in dwarf galaxies via other methods, such as the dwarf galaxy Henize 2-10 (Reines et al. 2011), have $W2-W3$ colours >4.2 ($W2-W3 \sim 5.0$ for Henize 2-10; Satyapal et al. 2014) and do not fall within the Jarrett et al. (2011) demarcation.

5. Verification using existing catalogues and optical line emission diagnostic

5.1. Existing catalogues

To verify the validity of our method, we compare our final list of AGN candidates with AGN candidates determined by other methods. The results of this comparison are listed below.

1. We find that 258 of the previously optically identified AGN in the MRBGD samples are also above our IR colour cut (see Fig. 1). Of the 43 that are not in the MRBGD samples, a literature search revealed that 16 had previously been identified as hosting an AGN (see Table 4), further supporting our IR colour selection criterion for a total of 276 out of 303 (or 91%) AGN candidates.

2. By splitting the MRBGD samples into type 1 (broad-line, hereafter BL) and type 2 (narrow-line, hereafter NL), we can see that type 1 AGN appear on average to have redder $W1-W2$ IR colours and lie preferentially above the IR cut-off, as compared to the type 2 AGN which lie preferentially below. This simply demonstrates what was discussed in Sect. 3 above, that the IR colour diagnostic does not exhaustively pick out AGN as their signatures can be washed out by an appreciable level of star-forming activity.

3. In Fig. 1, we highlight three famous Seyfert 1 galaxies, NGC 4395, POX 52, and UM 625, to show where they fall on the diagram (yellow circles). As discussed above, NGC 4395 has the only dynamical mass measurement of a CMBH in a dwarf galaxy (den Brok et al. 2015), POX 52 has a robust CMBH mass estimate (Barth et al. 2004) and UM 625 is

a Seyfert 1 galaxy hosting a low-mass CMBH (Jiang et al. 2013). It should be noted that UM 625 was added manually, and is not part of our sample as it is neither a dwarf nor nearby, though its low-mass CMBH still makes it an object of interest. We see that the AGN candidates for these three galaxies have colours above our selection cut-off.

4. It can be noted that there are four outliers with very red colours, i.e. $W1 - W2 > 1.7$, in the top right-hand corner of the diagram. Two of these (magenta circles in Fig. 1) are the low-metallicity and heavily obscured BCDs that were originally identified by Griffith et al. (2011) as already discussed above. These have been flagged in Table 2 as they are outliers and have optical diagnostics consistent with HII regions. The other two are HIPASS J1247-77 ($W1 - W2 \sim 2.086$) and NGC 5253 ($W1 - W2 \sim 1.757$), one of the nearest known BCDs. For these, we have no optical diagnostic information.

5. In Fig. 1, right, we show where the NED sample of BCD galaxies are located. BCDs are small, gas rich galaxies that are currently in a period of enhanced star formation. These galaxies are characterized by their blue colour, low metallicity and compact size. Some are extremely dusty (Griffith et al. 2011) (magenta circles found in the top left corner of Fig. 1, right) and appear to be dominated by star formation. Others, like MRK 709 S (red circle in Fig. 1, right), have X-ray and radio emission indicative of AGN activity (Reines et al. 2014). The WISE colours of MRK 709 S are $W1 - W2 = 0.323$ and $W2 - W3 = 4.010$, falling just below our colour cut. The fact that some of the BCDs do have signs of BH accretion activity indicates that the red colours may not be solely due to star formation in all cases.

5.2. Optical line emission diagnostic

We explored the distribution of our sample of 3326 galaxies with WISE matches and $S/N > 3$ in $W1$, $W2$ and $W3$ in the diagnostic diagrams of narrow-line ratios, which are powerful tools for distinguishing Seyfert galaxies, low-ionisation nuclear
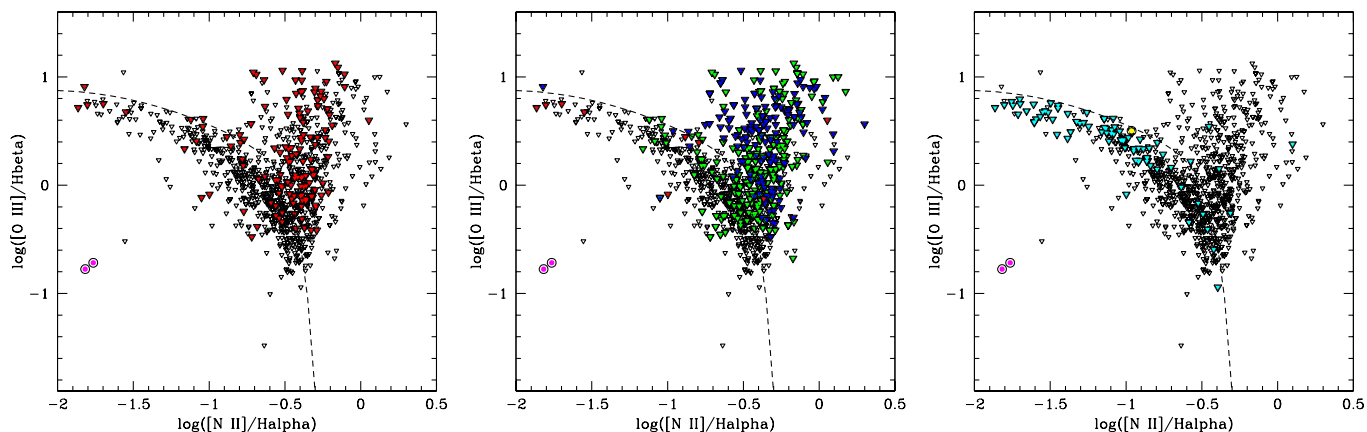
Fig. 3. *Left*: [OIII]/Hβ vs. [NII]/Hα diagnostic diagram for the 954 out of the 3326 galaxies with both line flux ratio measurements from the MPA/JHU catalogue. As in Fig. 1, the 135 sources above our IR colour cut are shown as red filled triangles. The dashed line is the demarcation line between normal star-forming galaxies and AGN from Stasinska et al. (2006). *Middle*: same as left, but showing the 126 AGN that were previously identified in the MRBGD optical samples split into 111 type 1 (BL; green filled triangles) and 16 type 2 (NL; blue filled triangles). One-third of this MRBGD sample are located in the region for HII galaxies. The 9 candidate AGN, selected using the IR diagnostic, which are not in the samples of MRBGD are shown as red filled triangles. *Right*: same as left, but showing the 83 BCDs (cyan filled triangles) and the two low-metallicity and heavily obscured BCDs that were originally identified by Griffith et al. (2011) (magenta filled circles). The BCD MRK 709 S (yellow filled circle), one of the most metal-poor BCDs with X-ray and radio emission indicative of AGN activity, is also located in the region for HII galaxies.

emission-line region sources, and HII galaxies (Baldwin et al. 1981; Veilleux & Osterbrock 1987; Ho et al. 1997; Kewley et al. 2001, 2006; Kauffmann et al. 2003). Diagnostic line-intensity ratios, such as [OIII]/Hβ and [NII]/Hα, corrected for reddening, are effective at separating populations with different ionisation sources. The ionising radiation field found in active galaxies is harder than in star-forming galaxies, and this gives higher values of [NII]/Hα and [OIII]/Hβ. Hence, the narrow line AGN are found in the upper right portion of the [OIII]/Hβ versus [NII]/Hα diagnostic diagram. The lines in these ratios are also selected to be close in wavelength space in order to minimize the effect of dust extinction on the computed line ratios.

We obtained emission line fluxes and stellar mass estimates for our sample from the Max Planck Institute for Astrophysics/Johns Hopkins University (MPH/JHU) collaboration[1], which contains 927552 SDSS galaxies. Of the 968 matches, we found that 954 (9 of the 43 AGN candidates without prior identification) had all four [OIII], Hβ, [NII], and Hα line fluxes and we were therefore able to compute the line-intensity ratios shown in Fig. 3, left. As in Fig. 1, left, our 135 nearby galaxies are shown as red triangles and the sample of 126 galaxies, including dwarfs, that had already been identified as having the optical spectroscopic signature of AGN activity (MRBGD) are shown as black open triangles. These additional optically identified AGN are split into 111 type 1 (BL; green filled triangles) and 16 type 2 (NL; blue filled triangles). The dashed line is the demarcation line between normal star-forming galaxies and AGN from Stasinska et al. (2006).

The main results of this comparison is summarized below.

1. As expected, the majority of the optically classified AGN are located in the conventional region of Seyfert galaxies, in terms of the semi-empirical demarcation line of Stasinska et al. (2006) (the dashed line in Fig. 3, left) in the [OIII]/Hβ versus [NII]/Hα diagram. This also includes four objects that had not previously been identified as AGN, if we

conservatively include the two objects close to the demarcation line (red triangles in Fig. 3, left).

2. The remaining one-third of the objects (five that had not previously been identified as AGN) are located in the region for HII galaxies in the same diagram. However, this does not necessarily mean that they are not AGN. Indeed, Sartori et al. (2015) compared AGN selected via three methods (using the classical BPT diagram, a similar optical emission line diagnostic based on the He II 4686 Å line, and mid-IR colour cuts) and found that only 3 of their 336 sources fulfilled all three criteria and that different criteria selected host galaxies with different physical properties such as stellar mass and optical colour. It is therefore likely that our IR colour cut is selecting a different subsample of AGN to that selected by the optical diagnostic diagram. Also, as is reported in Dong et al. (2012), this difference can be explained by the possible inclusion in the SDSS fibre aperture of emission from star formation regions in the host galaxies. Hence, although the optical spectra undeniably reveal the presence of a broad-line AGN, the narrow-line ratios may still be dominated by the characteristic emission of an HII region. We also note that MRK 709 S (red circle in Fig. 3, right), which has X-ray and radio emission indicative of AGN activity (Reines et al. 2014), is located very close to the demarcation line.

3. Our comparison reveals some possible issues regarding using the usual demarcation line between normal star-forming galaxies and AGN. Indeed, it is possible that the demarcation may not apply to the low-mass galaxy regime and for nearby galaxies. Given that the BPT diagram is empirically derived, and to date there has been little data on AGN in dwarfs, this is perhaps not surprising. In relation to this, it has also been known for some time that star formation behaves differently in some dwarf galaxies where there is a steepening of the Kennicutt–Schmidt law (Bigiel et al. 2008; Elmegreen et al. 2011; Roychowdhury et al. 2015). Additionally, recent work by Kewley et al. (2015) has shown that at high redshift, the demarcation line changes as a function of redshift. It is
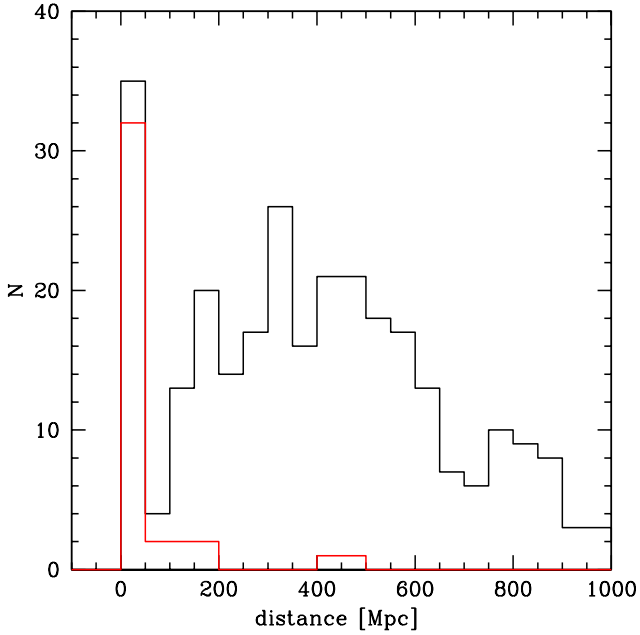
---

[1] http://www.mpa-garching.mpg.de/SDSS/

Fig. 4. Distance distribution of our IR selected sample of 300 AGN candidates with known redshift/distance. The subsample of 40 galaxies selected via the IR diagnostic, shown here in red, contains the nearest AGN candidates known today.

therefore perhaps possible that such a dependence could also extend to very low redshifts and/or low masses.

6. Distance distribution

One of the main goals of this study is to identify the closest dwarf galaxy hosting an AGN. Hundreds of active massive black hole candidates have already been detected at the centres of low-mass galaxies (e.g. Marleau et al. 2013; Moran et al. 2014; Reines et al. 2013). The major limitation of these works, however, is that they do not provide an unambiguous confirmation of the existence of these IMBHs as they rely solely on detecting the radiative signatures of AGN. Moreover, the dwarf galaxies in these existing samples are too far away to carry out dynamical studies (e.g. the Reines et al. 2013, sample has a redshift range of $z = 0.001-0.055$). It follows that in order to firmly establish that massive black holes do indeed exist at the centres of dwarf galaxies, it is absolutely necessary to extend our search to the very nearby Universe, i.e. to the galaxies for which we can resolve the sphere of influence of the CMBH and obtain dynamical mass estimates.

In Fig. 4 we show the distance distribution of the 300 out of the 303 galaxies with known redshift/distance. The first three candidates listed in Table 2 have no known redshift/distance. The sample of 40 galaxies selected via the IR diagnostic, shown in red, contains the nearest AGN candidates known today. Below 11 Mpc, we find 11 AGN candidates, including NGC 4395 (4.5 Mpc) which has been until now the closest one identified in a dwarf galaxy. Our method detected AGN in five galaxies that are closer than NGC 4395: HIPASS J1247-77 (3.2 Mpc), UGC 04459 (3.2 Mpc), NGC 5253 (3.6 Mpc), IC 2574 (3.8 Mpc) and CIRCINUS (4.2 Mpc). Of these, four can be classified as dwarf galaxies based on their stellar mass and/or absolute magnitude: HIPASS J1247-77 (Ryan-Weber et al. 2002) has a magnitude $M_B = -12.91$ (Karachentsev et al. 2004), UGC 04459 has a stellar mass of $\sim 9.7 \times 10^6$ $M_\odot$ and a magnitude $M_B = -13.43$

(Zhang et al. 2012), NGC 5253 (Turner et al. 2015) has a stellar mass of $\sim 1.5 \times 10^8$ $M_\odot$ (Martin 1998) and IC 2574 has stellar mass of $\sim 6.3 \times 10^7$ $M_\odot$ (Lee et al. 2011) and a magnitude $M_B = -16.8$ (Walter & Brinks 1999). The fifth galaxy, CIRCINUS, has a stellar mass of $\sim 9.5 \times 10^{10}$ $M_\odot$ and is therefore not considered a dwarf galaxy (For et al. 2012). In the context of being able to follow-up and confirm the presence of a IMBH in a dwarf galaxy with dynamical measurement, this implies that nearby dwarf galaxies should be targeted for dynamical observations.

7. Stellar mass estimates

We are interested in determining whether low-mass galaxies harbour a CMBH, and if so, whether or not the correlation between BH mass and total stellar mass derived in Marleau et al. (2013) extends to the low-mass regime. Therefore, in our calculation of stellar and BH masses, we did not only consider galaxies in our sample of dwarfs but also included the other galaxies in our nearby galaxies sample.

We used a combination of three independent methods to estimate the stellar masses for the 300 out of 303 galaxies with redshift measurement. The first method consisted of fitting the SEDs of our galaxies, constructed from SDSS photometry, using the MAGPHYS package (da Cunha et al. 2008). For the second method, we estimated the stellar masses following the empirical relation of Taylor et al. (2011, see their Eq. (8)). This method combines a galaxy's luminosity (M_i expressed in the AB system) with a mass-to-light ratio derived from a colour measurement ($g-i$). We transformed the SDSS magnitudes into AB mag, applied K-corrections using the method of Chilingarian et al. (2010), which, for the low-redshift ($z < 0.01$) galaxies in our sample, typically affect the g and i values by a few hundredths of a magnitude. The absolute magnitude M_i was computed using the distances given in Table 2. This method only applies for galaxies with $z < 0.5$ (297 of the 300 galaxies; all higher redshift sources are in the MRBGD samples). The third method consisted of using the Ks-band magnitude taken from both the PSC and the XSC of 2MASS. A general calibration factor was applied to the Ks fluxes by comparing the stellar masses to the SED derived stellar masses.

We compared the stellar masses measured from our three methods with those listed in the MPA/JHU and Mendel et al. (2014) catalogues and those found in the literature. For the 261 galaxies with stellar masses from both the SED fit and the color measurement method, we found in general very good agreement between the two estimates, with only two exceptions wherein the two mass estimates differ by an amount larger than the scatter. We find excellent agreement between our SED fit stellar masses and those of the MPA/JHU and Mendel et al. (2014) catalogues which confirms that our SED fit stellar mass estimates are robust. We also find in general good agreement between the SED fit stellar masses and the few stellar masses which were reported by MRBGD.

As can be seen in Fig. 5, we sample evenly a broad distribution of stellar masses, including dwarf galaxies in the stellar mass range $\sim 10^6-10^9$ $M_\odot$.

8. WISE/AGN fraction

As discussed in Introduction, dwarf galaxies exhibit many properties that distinguish them from massive galaxies (e.g. mass-to-light ratios, star formation histories, metallicities) and questions
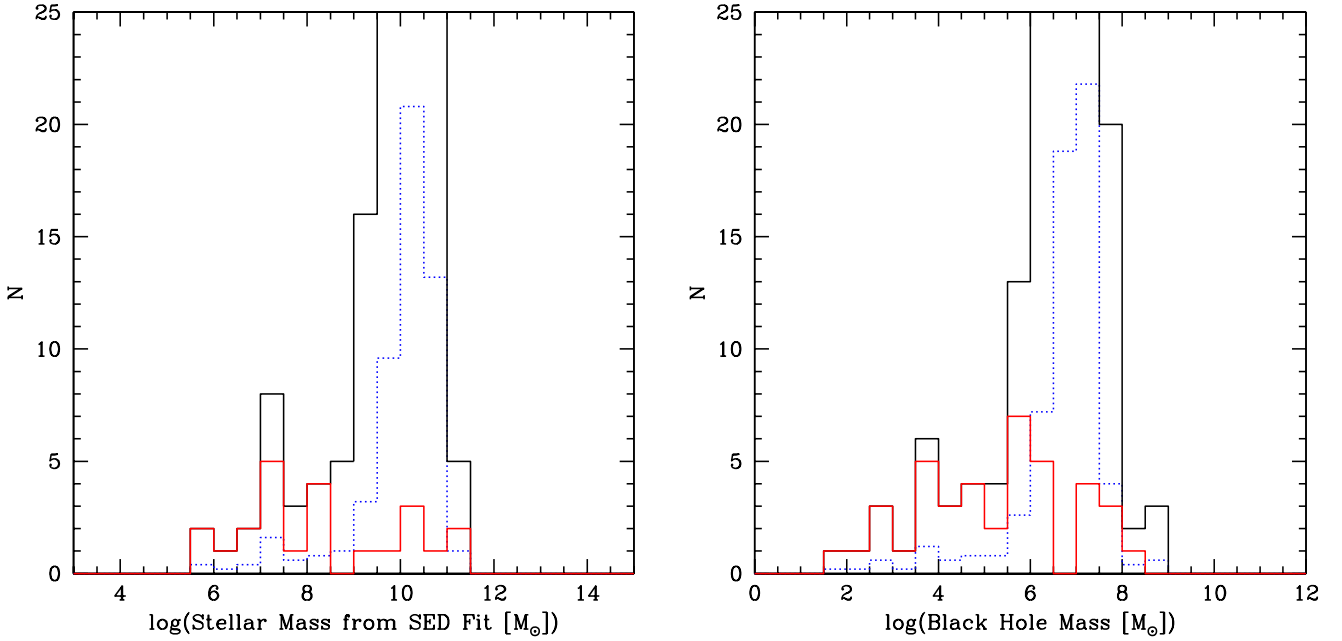
Fig. 5. *Left*: SED-based stellar mass distribution of our sample of 264 AGN candidates. The subsample of 23 galaxies that are not in the samples of MRBGD, shown here in red, contains the lowest stellar mass galaxies hosting an AGN candidate known today. The SED-based stellar mass distribution of our sample of 264 AGN candidates is also shown scaled down by a factor of 5 (blue dotted line). *Right*: black hole mass distribution of our sample of 300 AGN candidates with estimated black hole mass. The black hole masses were estimated from their IR luminosity, assuming $L_{bol} = 0.1 \, L_{Edd}$, the mean of our calibration sample. The subsample of 40 galaxies selected via the IR diagnostic, shown here in red, contains the lowest mass BH candidates known today. As in the left plot, the black hole mass distribution of our sample of 300 AGN candidates is also shown scaled down by a factor of 5 (blue dotted line).
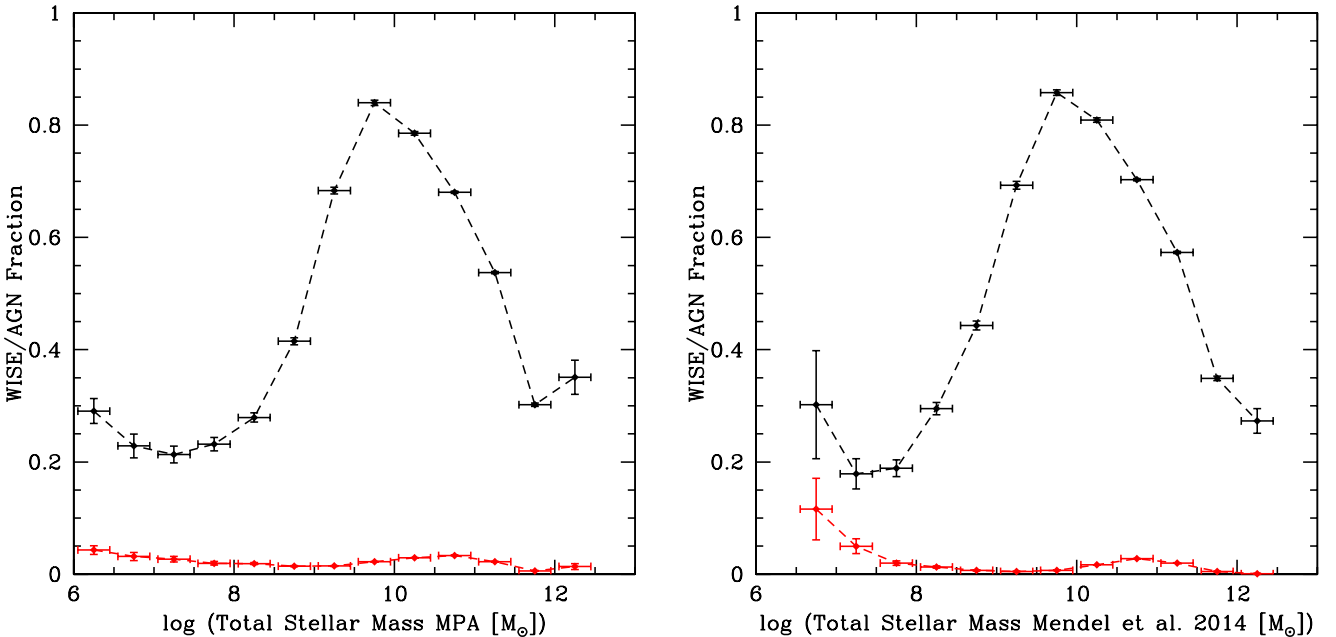
Fig. 6. *Left*: WISE (black curve)/AGN (red curve) fraction as a function of stellar mass derived from the MPA/JHU catalogue. *Right*: same as left but from the catalogue of Mendel et al. (2014).

exist about the nature of their evolution with respect to massive galaxies. In this regard, it is interesting to consider whether AGN have evolved differently in dwarf galaxies than in massive galaxies. A measure of this is given by the AGN fraction at a given time and mass.

Starting from the MPA/JHU catalogue of galaxies with stellar masses and from the catalogue of Mendel et al. (2014), we

examine the fraction of WISE matches and IR selected AGN as a function of stellar mass in each of these samples. Each catalogue was cross-matched independently to the WISE All-Sky Release Source Catalog using the same method as described in Sect. 3 and the same colour cut as described in Sect. 4. The errors were computed assuming Poisson statistics. As can be seen in Fig. 6, the fraction of IR selected AGN shows a signature
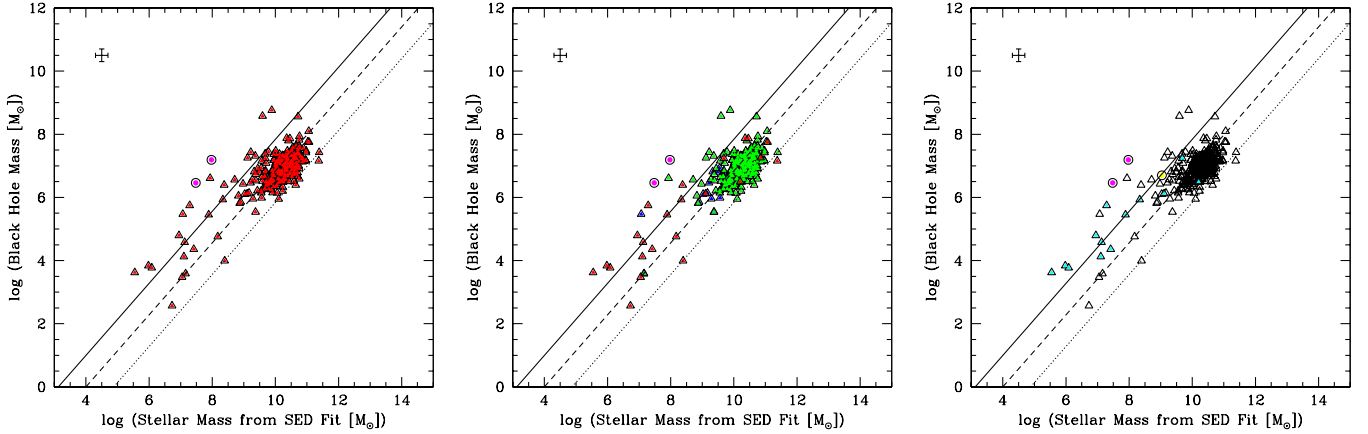
Fig. 7. *Left*: total stellar mass from SED fit vs. black hole mass obtained using the bolometric luminosity for our infrared sample of 264 galaxies with both known redshifts/distances and stellar masses (red filled triangles). The data points and bisector linear regression fit of Marleau et al. (2013) (dashed line) are plotted for $L_{bol}/L_{Edd} = 0.1$. Also shown are the fit for $L_{bol}/L_{Edd} = 1.0$ (dotted line) and for $L_{bol}/L_{Edd} = 0.01$ (solid line). *Middle*: same as left, but showing previously identified AGN of type 1 and type-2, respectively shown as green filled triangles and blue filled triangles, and the AGN candidates identified from the IR diagnostic only, shown as red filled triangles. Also shown are the two low-metallicity and heavily obscured BCDs that were originally identified by Griffith et al. (2011) (magenta filled circles). *Right*: same as left, but showing the BCDs (cyan filled triangles), the two low-metallicity and heavily obscured BCDs that were originally identified by Griffith et al. (2011) (magenta filled circles), and the BCD MRK 709 S with X-ray and radio emission indicative of AGN activity (yellow filled circle).

bump at a stellar mass $\sim 5.6 \times 10^{10}\ M_\odot$. Also, the fraction of AGN appears to increase as a function of decreasing stellar mass at stellar masses below $\sim 10^9\ M_\odot$, i.e. in the low-mass regime of dwarf galaxies, an effect also reported in Satyapal et al. (2014, see their Fig. 5). Note, however, as can also be seen in the figure, that this increase is accompanied by an increase in the WISE fraction. This is not the case for the bump seen at $\sim 5.6 \times 10^{10}\ M_\odot$, which is displaced from the peak in the WISE fraction. If real, this behaviour at low mass could be due to 1) the fact that BH accretion activity is higher in nearby dwarf galaxies than in their more massive counterparts (similar to the star-forming activity, i.e. the "downsizing" effect); 2) the fact that it is easier to detect WISE sources/AGN in nearby low-mass (low surface brightness) galaxies; or 3) the fact that at these low masses, the fraction of AGN candidates contaminated by star formation may be higher. This is a result that should be further explored and confirmed.

9. Black hole mass estimates

Black hole masses were estimated using the bolometric luminosity of our AGN candidates. Bolometric luminosities, taken to be the 100 μm to 10 keV integrated luminosity (Richards et al. 2006), are typically obtained using corrections to the mid-infrared bands where the AGN emission dominates. The 12 (W3) and 22 μm (W4) k-corrected flux densities from WISE can be used to compute the bolometric luminosities of the WISE colour-selected AGN by applying the bolometric corrections $L_{bol} \simeq 8 \times L_{12\ \mu m}$ (W3) and $L_{bol} \simeq 10 \times L_{22\ \mu m}$ (W4) from Richards et al. (2006), which are not strongly dependent on AGN luminosity (see their Fig. 12). However, note that Richards et al. (2006) only considered type 1 (BL) AGN in their analysis so that applying these corrections to type 2 AGN may lead to additional uncertainties in the BH mass estimates. Here, we only compute the BH mass estimates based on the 12 μm luminosities, as the S/N of the WISE data in the 12 μm images is higher than in the 22 μm images. By comparison, the bolometric luminosity of an AGN can also be estimated using the [O III] λ5007
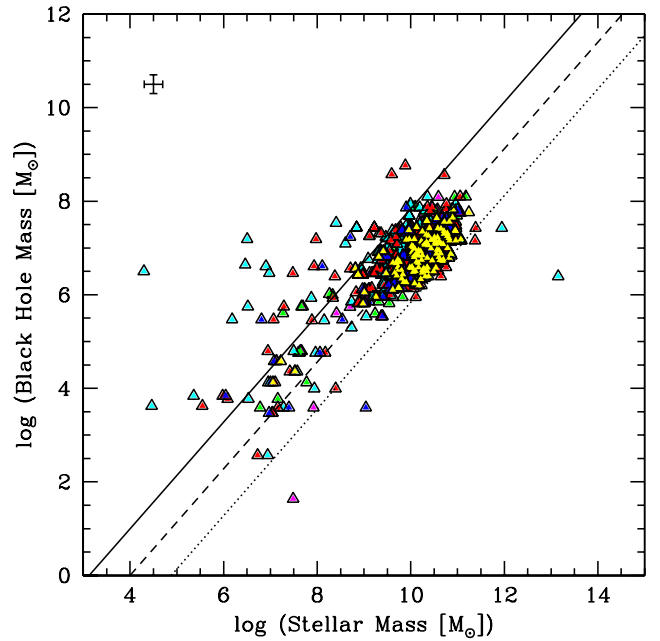

Fig. 8. Total stellar mass from all methods used for stellar mass measurements vs. black hole mass obtained using the bolometric luminosity for our infrared sample of 300 galaxies: from SED fit (red filled triangles), from colour measurement (cyan filled triangles), from Ks-band from 2MASS/PSC and XSC (magenta filled triangles), from the literature (blue filled triangles), from Mendel et al. (2014; yellow filled triangles) and MPA/JHU catalogues (green filled triangles).

emission line luminosity (e.g. Moran et al. 2014). In this case, the bolometric correction ranges from a factor of a hundred ($L_{bol} \simeq 3500 \times L_{5007}$) (Heckman et al. 2004) to a factor of ten ($L_{bol} \simeq 174 \times L_{5007}$) (Greene et al. 2007) larger than the IR bolometric correction.

For point source AGN candidates, we used the w3mpro magnitudes to compute BH masses. For our 30 extended source AGN candidates, we used the aperture magnitude corresponding to the

measured extent of the central source in W3 (e.g. for a galaxy with a radial extent of 19 arcsec in W3, we used w3mag_6). As 11 of our AGN candidates are spatially larger than the largest WISE aperture (24.75 arcsec radius aperture), the BH mass estimates for these sources is only a lower limit. Given the bolometric luminosity derived from the IR, making the assumption that accretion is at the Eddington limit yields a lower limit on the black hole mass. However, given that the growth rates of AGN can span several orders of magnitude, from super-Eddington accretion to 10^{-3} $L_{\rm Edd}$ (Simmons et al. 2013; Steinhardt & Elvis 2010), we computed black hole masses assuming the following three cases: $L_{\rm bol} = L_{\rm Edd}$, $L_{\rm bol} = 0.1$ $L_{\rm Edd}$ and $L_{\rm bol} = 0.01$ $L_{\rm Edd}$.

In a separate work (López 2015), the IR CMBH mass estimates were calibrated using 113 galaxies with robust CMBH mass measurements. Of the 113 galaxies, 51 have estimates based on the reverberation mapping method and 62 based on dynamical measurements. After following the procedure described in Sects. 3 and 4, 50 of these galaxies were identified as AGN candidates based on our IR colour diagnostic and their bolometric luminosity was computed as described in the paragraphs above. By comparing the CMBH mass estimates based on the other two methods to the estimate based on the IR method, the distribution of $L_{\rm bol}/L_{\rm Edd}$ was computed. A Gaussian fit to this distribution, in log space, yielded a mean of -1.0 and a σ of 0.6, in agreement with the range of Eddington ratios found in the literature (Woo & Urry 2002; Mushotzky et al. 2008).

The histogram of BH masses computed using $L_{\rm bol} = 0.1$ $L_{\rm Edd}$, the mean value derived from our calibration sample (-1.0 in log space), is shown in Fig. 5, right. This choice of $L_{\rm bol}/L_{\rm Edd}$ was also used in Marleau et al. (2013) and also appears to be a good fit to this data set (see Sect. 10). The black hole masses associated with the dwarf galaxies range from $\sim 10^3 - 10^6$ $M_\odot$ (see Sect. 10), which is a significantly lower range than has previously been probed. However, as stated above, note that the Eddington ratio is known to vary by as much as three orders of magnitudes for different AGN so our results are also presented for values of $L_{\rm bol}/L_{\rm Edd}$ equal to 0.01 and 1.0.

For NGC 4395, since an Eddington ratio has been measured with a value of 0.0012 (Peterson et al. 2005), we can compute its IR CMBH mass directly. We calculate a mass of 3.6×10^5 $M_\odot$, in very good agreement with the dynamical mass of 4×10^5 $M_\odot$ given by den Brok et al. (2015). POX 52 also has a reported Eddington ratio of $0.2-0.5$ (Thornton et al. 2008), which we can use to compute an IR CMBH mass. Using a ratio of 0.2, we obtain an IR CMBH mass of 2.0×10^5 $M_\odot$, in agreement with the range of CMBH masses of $2.2-4.2 \times 10^5$ $M_\odot$ obtained by Thornton et al. (2008) using other CMBH mass estimator methods.

10. BH mass versus stellar mass scaling relation

Using the stellar masses of the galaxies and the black hole masses estimated from the bolometric luminosity of the AGN candidate, we present in Fig. 7, left, the correlation between black hole mass and total SED stellar mass for our sample of 264 galaxies. We find active BH in nearby dwarfs, as well as in dwarf galaxies with lower stellar masses ($\sim 10^6 - 10^9$ $M_\odot$) and correspondingly lower BH masses ($\sim 10^3 - 10^6$ $M_\odot$) than the previous works of MRBGD, which only probed to $10^8 - 10^9$ stellar masses. We also find that the current results are consistent with the existing correlation (Marleau et al. 2013) extending linearly (in log-log space) into the lower mass regime. However, we cannot rule out with the current data that the correlation could be weakly non-linear in the low-mass regime.
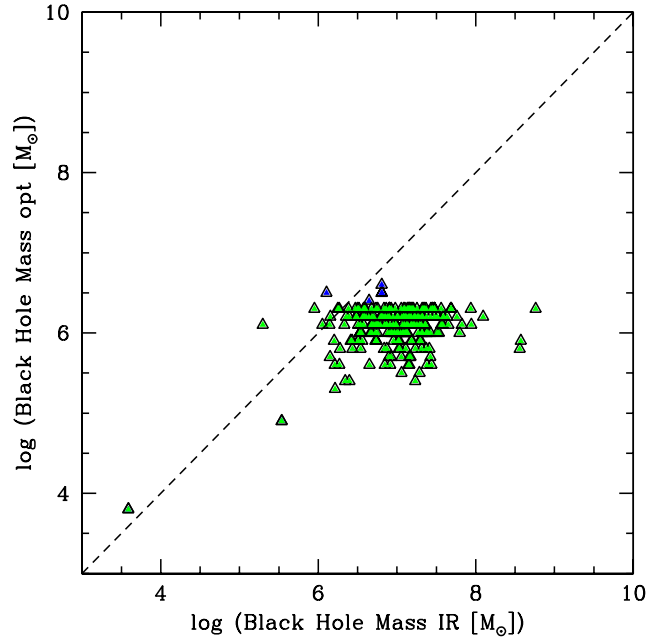
Fig. 9. Comparison between the black hole mass estimates computed from their IR luminosity and the black hole mass computed from the [OIII] $\lambda5007$ line flux from the works of MRBGD, for a subsample of 248 galaxies for which we were able to find a match (black open triangles). Previously optically identified type 1 and type 2 AGN are shown as green filled triangles and blue filled triangles, respectively.

In Fig. 7, middle, we examine the stellar mass versus BH mass relationship of the BCDs. We see that in the low-mass regime, the BCDs tend to be located mostly above the relation. This may indicate that a possible upturn at low mass is not real but due to contamination from star formation activity. Indeed, we find that the actively star-forming BCDs of Griffith et al. (2011) (magenta circles) fall above the relation. Also, the AGN hosting BCD MRK 709 S (Reines et al. 2014) (red circle) is expected to be affected by the host galaxy light based on its IR colour ($W1 - W2 = 0.323$). Its position in the diagram does indeed show a value slightly above the relation.

The errors on the stellar masses were determined using the uncertainties associated with the SED fit and were found to be of the order of 0.2 dex (97.5 percentile or 2σ error). In Fig. 8, we explore the effect of the uncertainty introduced by using different methods on the scatter of the stellar mass versus BH mass relation. The different colours are associated with the different methods and catalogues used in estimating the stellar masses. Except for the colour measurement method, we find that the agreement between the methods is quite good (see also Sect. 7) and does not significantly change the scatter seen in Fig. 7, left.

The errors on the BH mass were calculated from the uncertainties in the bolometric luminosity measurements and were found to be ~ 0.2 dex. However, the main source of uncertainty in this measurement is the value of $L_{\rm bol}/L_{\rm Edd}$, which we have assumed to be the same for all sources but instead most likely varies for each source. As can be seen in Fig. 7, simply allowing this value to vary from 0.01 to 1.0 reproduces most of the scatter seen in the data.

We compare in Fig. 9 the black hole mass estimates computed from the IR luminosity and those computed from the [OIII] $\lambda5007$ line flux from the works of MRBGD, for the subsample of 248 galaxies for which we were able to find a match. The BH mass cut-off of Greene et al. (2007) was 2×10^6 $M_\odot$

(6.3 in log space, see their Fig. 1) and this cut-off is easily seen in the diagram. Although some BH mass estimates are in agreement, the majority are not. The BH mass estimates computed from the [OIII] $\lambda 5007$ line flux are systematically lower than the BH mass estimates computed using the IR method.

11. Discussion and conclusions

We undertook a census of central massive black holes in the very nearby Universe, targeting specifically low-mass dwarf systems with BH masses in the IMBH mass range. Additionally, we were interested in detecting AGN in nearby galaxies regardless of their mass so that we could identify targets for future dynamical mass measurement. The results of our paper are as follows:

1. Using the WISE All-Sky Release Source Catalog, we examined the IR colours of a sample of known low-mass and other nearby systems in order to identify candidate AGN by applying the infrared colour diagnostic $W1 - W2 > 0.5$. We find that 303 nearby galaxies have WISE colours consistent with galaxies containing an AGN.

2. We validate our IR detection method. Of the 303 candidate AGN, 276 (or 91%) are subsequently found to have been independently identified as AGN via other methods. The remaining 9% require follow-up observations to confirm that their red IR colours ($W1 - W2 > 0.5$) are not due to star formation. We find that if we applied an additional cut in $W2 - W3$ colour, e.g. $W2 - W3 < 4.2$, we would reject 16 AGN candidates, 8 of which are optically identified AGN (2 type 1 and 6 type 2) and only 2 are known low-metallicity and heavily obscured BCDs. The remaining 6 have colours similar to these 8 optically identified AGN and hence are valid candidate AGN. We also point out that AGN detected via other methods in dwarf galaxies, such as the dwarf galaxy Henize 2-10, have $W2 - W3$ colours >4.2 ($W2 - W3 \sim 5.0$) and do not fall within the Jarrett et al. (2011) demarcation.

3. We verify our IR detection of AGN candidates by comparing the data with existing catalogues and optical line emission diagnostics. We find that type 1 AGN appear on average to have redder $W1 - W2$ IR colours and lie preferentially above the IR cut-off, as compared to the type 2 AGN which lie preferentially below. We show that NGC 4395, POX 52 and UM 625 have WISE colours above our selection cut-off. We point out that although some low-metallicity and extremely obscured BCDs have very red colours, others are not so red, such as MRK 709 S with $W1 - W2 = 0.323$ and $W2 - W3 = 4.010$.

4. We find that 11 of our candidate AGN lie within a distance of 11 Mpc and are the nearest AGN candidates known today. Based on our stellar mass cut, we also find that our AGN candidate sample contains 62 dwarf galaxies.

5. Using a combination of three independent methods, we obtain stellar masses for the galaxies in our AGN candidate sample in the range $\sim 10^6 - 10^{11}\ M_\odot$, extending far beyond the dwarf galaxy mass demarcation.

6. We show that the fraction of IR selected AGN shows a signature bump at a stellar mass $\sim 5.6 \times 10^{10}\ M_\odot$. Also, the fraction of AGN appears to increase as a function of decreasing stellar mass at stellar masses below $\sim 10^9\ M_\odot$, i.e. in the low-mass regime of dwarf galaxies.

7. Black hole masses are estimated using the bolometric luminosity of the AGN candidates and computed for three cases of bolometric-to-Eddington luminosity ratio. Using the previously measured Eddington ratio of 0.0012, we calculate for NGC 4395 an IR CMBH mass of $3.6 \times 10^5\ M_\odot$, in agreement with the recently measured dynamical mass estimate of $4 \times 10^5\ M_\odot$. Similarly, using a previously measured Eddinton ratio of 0.2, we compute for POX 52 an IR CMBH mass of $2.0 \times 10^5\ M_\odot$, in agreement with the mass range of $2.2 - 4.2 \times 10^5\ M_\odot$ obtained using other methods.

8. Assuming all of our candidates are AGN, we find that activity is detected in dwarf galaxies with stellar masses from approximately 10^6 to $10^9\ M_\odot$ and that this activity is due to black holes with masses in the range $\sim 10^3 - 10^6\ M_\odot$, assuming $L_{\rm bol} = 0.1\ L_{\rm Edd}$, the mean of our calibration sample. The black hole masses probed here are several orders of magnitude smaller than previously reported for centrally located massive black holes.

9. We examine the stellar mass versus black hole mass relationship in this low galaxy mass regime. The current results are consistent with the existing correlation extending linearly (in log-log space) into the lower mass regime. However, we cannot rule out with the current data that the correlation could be weakly non-linear in the low-mass regime.

These results suggest that central massive black holes are present in low-mass galaxies and in the Local Universe, and provide new impetus for follow-up dynamical studies of quiescent black holes in local dwarf galaxies.

References

Alonso-Herrero A., Pereira-Santaella, M., Rieke, G. H., et al. 2014, ApJ, 765, 78
Antonucci, R. 1993, ARA&A, 31, 473
Assef, R. J., Kochanek, C. S., Brodwin, M., et al. 2010, ApJ, 713, 970
Baldwin, J. A., Phillips, M. M., & Terlevich, R. 1981, PASP, 93, 5
Ballantyne, D. R., Draper, A. R., Madsen, K. K., Rigby, J. R., & Treister, E. 2011, ApJ, 736, 56
Bardeen, J. M. 1970, Nature, 226, 64
Barth, A. J., Ho, L. C., Rutledge, R. E., & Sargent, W. L. W. 2004, ApJ, 607, 90
Barth, A. J., Greene, J. E., & Ho, L. C. 2008, AJ, 136, 1179
Beifiori, A., Courteau, S., Corsini, E. M., et al. 2012, MNRAS, 419, 2497
Bender, R., & Kormendy, J. 2003, in Astronomy, Cosmology, and Fundamental Physics, Proc. of the ESO/CERN/ESA Symp. (Springer Verlag), 262
Benson, A. J. 2010, Phys. Rep., 495, 33
Bigiel, F., Leroy, A., Walter, F., et al. 2008, AJ, 136, 2846
Booth, C. M., & Schaye, J. 2009, MNRAS, 398, 53
Boselli, A., Lequeux, J., & Gavazzi, G. 2004, A&A, 428, 409
Bukhmastova, Y. L. 2001, Astron. Rep., 45, 581
Calzetti, D. 2011, PAHs and the Universe, eds. C. Joblin, & A. G. G. M. Tielens, EAS Pub. Ser., 46, 133
Chilingarian, I. V., Melchior, A.-L., & Zolotukhin, I. Y. 2010, MNRAS, 405, 1409
Comastri, A., Setti, G., Zamorani, G., & Hasinger, G. 1995, A&A, 296, 1
da Cunha, E., Charlot, S., & Elbaz, D. 2008, MNRAS, 388, 1595
Davis, B., Berrier, J. C., Johns, L., et al. 2014, ApJ, 789, 124
Dunn, J. 2010, MNRAS, 408, 392
DeGraf, C., Di Matteo, T., Khandai, N., & Croft, R. 2012, ApJ, 755, LL8
den Brok, M., Seth, A. C., Barth, A. J., et al. 2015, ApJ, 809, 101
Di Matteo, T., Springel, V., & Hernquist, L. 2005, Nature, 433, 604
Di Matteo, T., Colberg, J., Springel, V., Hernquist, L., & Sijacki, D. 2008, ApJ, 676, 33
Dong, X.-B., Wang, T., Yuan, W., et al. 2007, ApJ, 657, 700
Dong, X.-B., Ho, L. C., Yuan, W., et al. 2012, ApJ, 755, 167
Draine, B. T., Dale, D. A., Bendo, G., et al. 2007, ApJ, 633, 866
Elmegreen, B. G. 2011, EAS Pub. Ser., 51, 3
Engelbracht, C. W., Gordon, K. D., Rieke, G. H., et al. 2005, ApJ, 628, 29
Engelbracht, C. W., Rieke, G. H., Gordon, K. D., et al. 2008, ApJ, 685, 678

Fabian, A. C. 2012, ARA&A, 50, 455
Fan, X., Narayanan, V. K., Lupton, R. H., et al. 2001, AJ, 122, 2833
Ferrarese, L., & Merritt, D. 2000, AJ, 539, L9
For, B.-Q., Koribalski, B. S., & Jarrett, T. H. 2012, MNRAS, 425, 1934
Galliano, F., Madden, S. C., Jones, A. P., Wilson, C. D., & Bernard, J.-P. 2005, A&A, 434, 867
Galliano, F., Dwek, E., & Chanial, P. 2008, ApJ, 672, 214
Gebhardt, K., Bender, R., Bower, Gary, et al. 2000, AJ, 539, 13
Georgiev, I. Y., Böker, T., & Leigh, N. 2016, MNRAS, 457, 2122
Gordon, K. D., Engelbracht, C. W., Rieke, G. H., et al. 2008, ApJ, 682, 336
Greene, J. E., & Ho, L. C. 2004, ApJ, 610, 722
Greene, J. E., & Ho, L. C. 2007, ApJ, 670, 92
Griffith, R. L., Tsai, C.-W., Stern, D., et al. 2011, ApJ, 736, L22
Haider, M., Steinhauser, D., Vogelsberger, M., et al. 2016, MNRAS, 457, 3024
Heckman, T. M., & Kauffmann, G. 2011, Science, 333, 182
Heckman, T. M., Kauffmann, G., Brinchmann, J., et al. 2004, ApJ, 613, 109
Ho, L. C., Filippenko, A. V., & Sargent, W. L. W. 1997, ApJS, 112, 315
Ho, L., Kormendy, J., & Murdin, P. 2000, in Encyclopedia of Astronomy and Astrophysics, ed. P. Murdin (Bristol: Institute of Physics Publishing)
Hogg, D. W., Tremonti, C. A., Blanton, M. R., et al. 2005, ApJ, 624, 162
Ishibashi, W., & Fabian, A. C. 2014, MNRAS, 441, 1474
Jarrett, T. H., Cohen, M., Masci, F., et al. 2011, ApJ, 735, 112
Jiang, N., Ho, L. C., Dong, X.-B., Yang, H., & Wang, J. 2013, ApJ, 770, 3
Karachentsev, I. D., Karachentseva, V. E., Huchtmeier, W. K., & Makarov, D. I. 2004, AJ, 127, 2031
Karachentsev, I. D., Makarov, D. I., & Kaisina, E. I. 2013, AJ, 145, 101
Kauffmann, G., Jeckman, T. M., Tremonti, C., et al. 2003, MNRAS, 346, 1055
Kewley, L. J., Dopita, M. A., Sutherland, R. S., Heisler, C. A., & Trevena, J. 2001, ApJ, 556, 221
Kewley, L. J., Groves B., Kauffmann, G., & Heckman, T. 2006, MNRAS, 372, 961
Kewley, L. J., Zahid, H. J., Geller, M. J., et al. 2015, ApJ, 812, 20
Khalatyan, A., Cattaneo, A., Schramm, M., et al. 2008, MNRAS, 387, 13
King, A. 2003, ApJ, 596, L27
Koulouridis, E. 2014, A&A, 570, A72
Kormendy, J., & Ho, L. C. 2013, ARA&A, 51, 511
Kormendy, J., & Richstone, D. 1995, ARA&A, 33, 581
Lacy, M., Storrie-Lombardi, L. J., Sajina A., Appleton, et al. 2004, ApJS, 154, 166
Lacy, M., Petric, A. O., Sajina A., et al. 2007, AJ, 133, 186
Lee, J. C., Gil de Paz A., Kennicutt R. C. Jr., et al. 2011, ApJS, 192, 6
López, K. M. 2015, Master's Thesis, University of Innsbruck, Austria
Lynden-Bell, D. 1969, Nature, 223, 690
Lynden-Bell, D., & Rees, M. J. 1971, MNRAS, 152, 461
Ma, X., Hopkins, P. F., Faucher-Giguere, C. A., et al. 2016, MNRAS, 456, 2140
Madden, S. C., Galiano, F., Jones, A. P., & Sauvage, M. 2006, A&A, 446, 877
Magorrian, J., Tremaine, S., Richstone, D., et al. 1998, AJ, 115, 2285
Marble, A. R., Engelbracht, C. W., van Zee L., et al. 2010, ApJ, 715, 506
Marleau, F. R., Clancy, D., & Bianconi, M. 2013, MNRAS, 435, 3085
Marleau, F. R., Clancy, D., Bianconi, M., & Habas, R. 2014, MNRAS, submitted [arXiv:1411.3844]
Martin, C. L. 1998, ApJ, 506, 222
Mateo, M. 1998, ARA&A, 36, 435
Matsuoka, Y., Onoue, M., Kashikawa, N., et al. 2016, ApJ, 828, 26
McConnachie, A. W. 2012, AJ, 144, 4
McConnell, N., & Chung-Pei, M. 2013, ApJ, 764, 184
McKernan, B., Ford, K. E. S., Reynolds, C. S., et al. 2010, MNRAS, 407, 2399
McNamara, B. R., & Nulsen, P. E. J. 2007, ARA&A, 45, 117
Mendel, J. T., Simard, L., Palmer, M., Ellison, S. L., & Patton, D. R. 2014, ApJS, 210, 3

Merloni, A. 2015, Astrophysical Black Holes, Lect. Notes Phys. (Springer Int. Pub.), 905, 101
Merritt, D., & Ferrarese, L. 2001, ApJ, 547, 140
Moran, E., Shahinyan, K., Sugarman, H. R., Vélez, D. O., & Eracleous, M. 2014, AJ, 148, 22
Mortlock, D. J., Warren, S. J., Venemans, Bram P., et al. 2011, Nature, 474, 616
Muñoz-Mateos, J. C., Gil de Paz, A., Boissier, S., et al. 2009, ApJ, 701, 1965
Mushotzky, R. F., Winter, L. M., McIntosh, D. H., & Tueller, J. 2008, ApJ, 684, L65
Newton, R. D. A., & Kay, S. T. 2013, MNRAS, 434, 3606
Panessa, R., Bassani, L., Cappi, M., et al. 2006, A&A, 455, 173
Peirani, S., Jung, I., Silk, J., & Pichon, C. 2012, MNRAS, 427, 2625
Peterson, B. M. 2008, New Astron. Rev., 52, 240
Peterson, B. M., Bentz, M. C., Desroches, L.-B., et al. 2005, ApJ, 632, 799
Peterson, B. M., Somerville, R. S., & Storchi-Bergmann, T. 2010, Co-evolution of Central Black Holes and Galaxies (IAU S267), eds. B. M. Peterson , R. S. Somerville & T. Storchi-Bergmann (Cambridge, UK: Cambridge University Press)
Power, C., Nayakshin, S., King, A. 2011, MNRAS, 412, 269
Reines, A. E., Sivakoff, G. R., Johnson, K. E., & Brogan, C. L. 2011, Nature, 470, 66
Reines, A. E., Greene, J. E., & Geha, M. 2013, ApJ, 775, 116
Reines, A. E., Plotkin, R. M., Russell, T. D. et al. 2014, ApJ, 787, L5
Richards, G. T., Lacy, M., Storrie-Lombardi, L. J., et al. 2006, ApJS, 166, 470
Rosenberg, J. L., Ashby, M. L. N., Salzer, J. J., & Huang, J.-S. 2006, ApJ, 636, 742
Roychowdhury, S., Chengalur, J. N., Begum, A., & Karachentsev, I. D. 2009, MNRAS, 397, 1435
Ryan-Weber, E., Koribalski, B. S., Staveley-Smith, L., et al. 2002, AJ, 124, 1954
Salpeter, E. E. 1964, ApJ, 140, 796
Sargsyan, L., Smail, I., Moran, S. M., et al. 2011, ApJ, 730, 19
Sartori, L. F., Schawinski, K., Treister E., et al. 2015, MNRAS, 454, 3722
Satyapal, S., Secrest, N. J., McAlpine, W., et al. 2014, ApJ, 784, 113
Schawinski, K. 2012 , ArXiv e-prints [arXiv:1206.2661]
Seth, A. C., van den Bosch, R., Mieske, S., et al. 2014, Nature, 513, 398
Sijacki, D., Springel, V., Di Matteo, T., & Hernquist, L. 2007, MNRAS, 380, 877
Silk, J. 2013, ApJ, 772, 112
Silk, J., & Rees, M. J. 1998, A&A, 331, L1
Simmons, B. D., Lintott, C., Schawinski, K., et al. 2013, MNRAS, 429, 2199
Springel, V., Di Matteo, T., & Hernquist, L. 2005, MNRAS, 361, 776
Stasinska, G., Fernandes, R. C., Mateus, A., Sodre, L., & Asari, N. V. 2006, MNRAS, 371, 972
Steinhardt, C. L., & Elvis M. 2010, MNRAS, 402, 2637
Stern, D., Daddi, E., Béthermin, M., et al. 2012, ApJ, 753, 30
Taylor, E. N. 2011, MNRAS, 418, 1587
Thornton, C. E., Barth, A. J., Ho, L. C., et al. 2008, ApJ, 689, 892
Turner, J. L., Beck, S. C., Benford, D. J., et al. 2015, Nature, 519, 331
Treister, E., Urry, C. M., Chatzichristou, E., et al. 2004, ApJ, 616, 123
Urry, C. M., & Padovani, P. 1995, PASP, 107, 803
Veilleux, S., & Osterbrock, D. E. 1987, ApJS, 63, 295
Veron-Cetty, M. P., & Vernon, P. 2010, A&A, 518, A10
Walter, F., & Brinks, E. 1999, AJ, 118, 273
Woo, J.-H., & Urry, C. M. 2002, ApJ, 579, 530
Wright, E. L., Eisenhardt, P. R. M., Mainzer, A. K., et al. 2010, AJ, 140, 1868
Wu, Y., Charmandaris, V., Hao, L., et al. 2006, ApJ, 639, 157
Wu, X.-B., Wang, F., Fan, X., et al. 2015, Nature, 518, 512
Wurster, J., & Thacker, R. J. 2013, MNRAS, 431, 2513
Zel'dovich, Y. B., & Novikov, I. D. 1965, Sov. Phys. Doklady, 9, 834
Zhang, H.-X., Hunter, D. A., Elmegreen, B. G., Gao Y., & Schruba A. 2012, AJ, 143, 47
Zhao, J.-H., Anantharamaiah, K. R., Goss, W. M., et al. 1997, ApJ, 482, 186